High Ratio Bidirectional DC-DC Converter with a Synchronous Rectification H-Bridge for Hybrid Energy Sources Electric Vehicles

Yun Zhang[†], Yongping Gao[*], Jing Li[**], Mark Sumner[***], Ping Wang[*], and Lei Zhou[*]

[†,*]School of Electrical Engineering and Automation, Tianjin University, Tianjin, China
[**]Department of Electrical and Electronic Engineering, University of Nottingham, Ningbo, China
[***]Department of Electrical and Electronic Engineering, University of Nottingham, Nottingham, UK

Abstract

In order to match the voltages between high voltage battery stacks and low voltage super-capacitors with a high conversion efficiency in hybrid energy sources electric vehicles (HESEVs), a high ratio bidirectional DC-DC converter with a synchronous rectification H-Bridge is proposed in this paper. The principles of high ratio step-down and step-up operations are analyzed. In terms of the bidirectional characteristic of the H-Bridge, the bidirectional synchronous rectification (SR) operation is presented without any extra hardware. Then the SR power switches can achieve zero voltage switching (ZVS) turn-on and turn-off during dead time, and the power conversion efficiency is improved compared to that of the diode rectification (DR) operation, as well as the utilization of power switches. Experimental results show that the proposed converter can operate bidirectionally in the wide ratio range of 3~10, when the low voltage continuously varies between 15V and 50V. The maximum efficiencies are 94.1% in the Buck mode, and 93.6% in the Boost mode. In addition, the corresponding largest efficiency variations between SR and DR operations are 4.8% and 3.4%. This converter is suitable for use as a power interface between the battery stacks and super-capacitors in HESEVs.

Key words: Bidirectional DC-DC converter, HESEVs, H-bridge, High ratio, Synchronous rectification

I. INTRODUCTION

With the aggravation of the global energy crisis and the deterioration of the environmental pollution, clean-energy vehicles which are powered by renewable energy sources with reduced or zero pollution, are a new trend for the future of transportation [1]-[3]. While electric vehicles, e.g. fuel cell vehicles and pure electric vehicles, are one of the most significant types of clean-energy vehicles [4], [5]. These new energy vehicles reduce the consumption of non-renewable energy sources and results in pollution reduction [6]. However, high specific energy sources, such as fuel cell stacks and battery stacks cannot supply instantaneous power well for acceleration [7], [8]. In addition, the

battery stacks cannot store braking energy efficiently to extend mileage by a few seconds [9], [10]. Therefore, hybrid energy sources vehicles comprised of high specific energy and high specific power sources, e.g. battery stacks and super-capacitors, have been proposed by some scholars to fulfill the bidirectional stable energy and instantaneous power requirements for the high voltage DC-link of electric driving systems [11], [12].

Regarding high specific power sources (e.g. super-capacitors), they still have characteristics such as a low output voltage and a high output current [13]. In addition, their terminal voltages vary a great deal when they are being charged or discharged. Therefore, the high specific power sources are difficult to be directly parallel with the high voltage DC-link. And it is necessary to interface with the super-capacitors and the high voltage DC-link by a high ratio bidirectional DC-DC converter. The present high ratio bidirectional DC-DC converters can generally achieve high step-down and step-up voltages by high-frequency transformers, coupled inductors, or switched capacitors

[14]-[16]. However, the leakage of the transformer and the coupled inductors may easily induce higher voltage stresses across the power switches. In addition, the design parameters of the transformer and the coupled inductors would be affected by the leakage, and the magnetic components have to be off-standard. Particularly, it highly depends on the magnetic components and switched capacitors which would be subject to lower power density and non-easy packages, and may not be tolerant in HESEVs.

In fact, a synthesis method to achieve high ratio step-down and step-up DC-DC converters without coupled inductors or switched capacitors was proposed in [17], and the peak current loss due to the extreme duty cycles was reduced. However, compared with two-phase or three-level DC-DC converters, the high ratio unidirectional converters above operate with a lower efficiency [18], because the total inductor current flows simultaneously through two semiconductors, or the semiconductors have a full blocking voltage. In this paper, a high ratio bidirectional DC-DC converter with a H-Bridge is proposed to avoid the transformers, coupled inductors and switched capacitors. Furthermore, the high ratio bidirectional H-Bridge DC-DC converter with synchronous rectification operation is presented which takes full advantage of the power switches without any other hardware and improves efficiency, as the four driving circuits are actually needed for the bidirectional operation of the H-Bridge. The remainder of this paper is organized as follows. In Section II, the topology and operation principles of the proposed converter are stated. Then, some experimental results and analysis are given in Section III. Finally, the conclusion is delivered in Section IV.

II.   HIGH RATIO BIDIRECTIONAL CONVERTER AND OPERATIONS

A. Bidirectional Topology

The proposed high ratio bidirectional DC-DC converter with a SR H-Bridge is shown in Fig. 1. L is the energy storage/filter inductor, and C_{high} and C_{low} are the energy storage/filter capacitors. When energy flows from the high voltage side (U_{high}) to the low voltage side (U_{low}), the output voltage U_{low} is stepped down (in Buck mode) from U_{high} by controlling the power switches of Q_{D1}, and Q_{D4}, and the anti-parallel diodes of Q_{D2} and Q_{D3}. Otherwise, U_{high} is stepped up (in Boost mode) from U_{low} through the controlled power switches Q_{D2}, and Q_{D3}, as well as the anti-parallel diodes of Q_{D1} and Q_{D4}.

B. High Ratio Step-Down Operation

In terms of the step-down operation of the bidirectional H-Bridge shown in Fig. 1, its output voltage U_{low} is filtered from the PWM voltage U_{ab} by L and C_{low}, and U_{ab} can be described as:
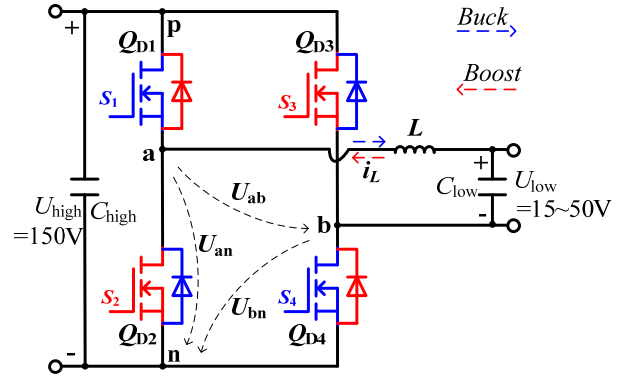
$$U_{ab} = U_{an} - U_{bn} \tag{1}$$

Fig. 1. High ratio bidirectional DC-DC converter with SR H-Bridge.

where U_{an} and U_{bn} are the output PWM voltage of the left and right half bridges, respectively. However, the high ratio step-down operation of this Buck DC-DC converter requires a narrow pulse voltage U_{ab}. In this paper, the narrow pulse voltage U_{ab} is obtained from the PWM voltage difference between the wider pulse voltages U_{an} and U_{bn}, by means of (1). Its high ratio step-down operation principle is shown in Fig. 2. The gate signal S_1 for the power switch Q_{D1} is decided by the modulation index m_b, as shown in Fig. 2(a) and 2(b). Similarly, the gate signal S_4 for the power switch Q_{D4} depends on the modulation index m_a, as shown in Fig. 2(a) and 2(c). In addition, it is under the conditions of $0<m_b<0.5<m_a<1$, and $m_a+m_b>1$. Therefore, the output PWM voltages U_{an} and U_{bn} are controlled by the gate signals S_1 and S_4, as shown in Fig. 2(d) and 2(e), and the narrow pulse voltage U_{ab} can be obtained by adjusting m_a and m_b which can be near 0.5.

In the current continuous mode, the energy stored in the inductor L is equal to the energy transferred to the load in each carrier period T, then it can be obtained that:

$$
\begin{aligned}
(U_{high} &- U_{low}) \times [(0.5T - t_{off4}) + (0.5T - t_{off1})] \\
&= U_{low} \times (t_{off1} + t_{off4})
\end{aligned} \tag{2}
$$

where t_{off1} and t_{off4} are the turn-off times for Q_{D1} and Q_{D4}, respectively. Then the step-down ratio M_{Buck} of the Buck DC-DC converter is obtained by:

$$
\begin{cases}
M_{Buck} = \dfrac{U_{low}}{U_{high}} = d_1 + d_4 - 1 \\
d_1 = 1 - m_b \\
d_4 = m_a
\end{cases} \tag{3}
$$

where d_1 and d_4 are the duty cycles of Q_{D1} and Q_{D4}, respectively. In addition, the relationship between M_{Buck} and m_a, m_b can be written as:

$$M_{Buck} = \frac{U_{low}}{U_{high}} = m_a - m_b, \ (0<m_b<0.5<m_a, \text{ and } m_a+m_b>1) \tag{4}$$

C. High Ratio Step-Up Operation

Regarding the step-up operation of the H-Bridge shown in Fig. 1, the output voltage U_{high} is obtained by rectifying the
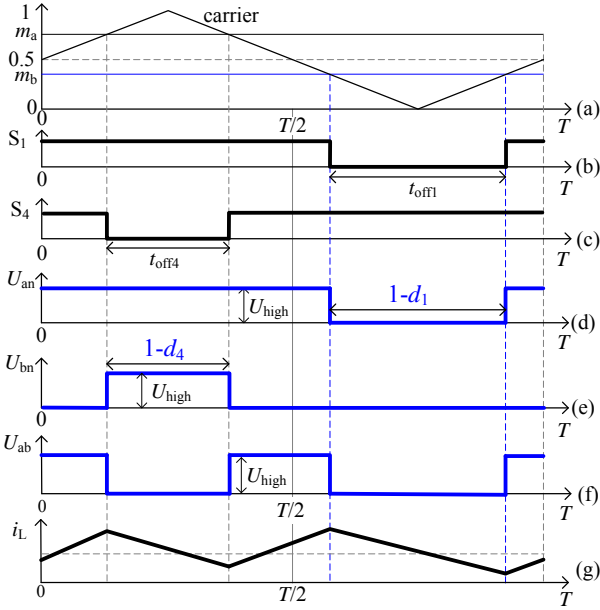
Fig. 2. High ratio step-down operation principle of H-Bridge.

Fig. 3. High ratio step-up operation principle of H-Bridge.

PWM voltage U_{ab} through the anti-parallel diodes of Q_{D1} and Q_{D4}, and the filter capacitor C_{high}. Thus, the high ratio step-up operation of the H-Bridge also needs a narrow pulse voltage U_{ab}, which is also obtained from the PWM voltage difference between the PWM voltages U_{an} and U_{bn}. Its operation principle is shown in Fig. 3. And the gate signals S_2 and S_3 for Q_{D2} and Q_{D3}, shown in Fig. 3(a-c), are generated by the modulation indices m_c and m_d, respectively. Furthermore, this is done under the conditions of $0<m_d<0.5<m_c<1$ and $m_c+m_d<1$. Therefore, the output PWM voltages U_{an} and U_{bn} of each half bridge are controlled by S_2 and S_3, as shown in Fig. 3(d) and (e). Finally, the narrow pulse voltage U_{ab} can be obtained by adjusting m_c and m_d, which can also be around 0.5.

Similarly, in the current continuous mode, the energy stored in the inductor L is equal to the energy transferred to the load in each carrier period T, then it can be obtained that:

$$(U_{high}-U_{low})\times[(0.5T-t_{on2})+(0.5T-t_{on3})] \\ =U_{low}\times(t_{on2}+t_{on3}) \tag{5}$$

where t_{on2} and t_{on3} are the turn-on times for Q_{D2} and Q_{D3}, respectively. As a result, the step-up ratio M_{Boost} of the H-Bridge can be obtained by means of (5) and Fig. 3(b), 3(c), and 3(g).

$$\begin{cases} M_{Boost}=\dfrac{U_{high}}{U_{low}}=\dfrac{T}{T-(t_{on2}+t_{on3})}=\dfrac{1}{1-(d_2+d_3)} \\ d_2=1-m_c \\ d_3=m_d \end{cases} \tag{6}$$

where d_2 and d_3 are the duty cycles of Q_{D2} and Q_{D3}, respectively. Then, the relationship between M_{Boost} and m_c and m_d can be described as:

$$M_{Boost}=\dfrac{U_{high}}{U_{low}}=\dfrac{1}{m_c-m_d},\ (0<m_d<0.5<m_c,\ \text{and}\ m_c+m_d<1) \tag{7}$$

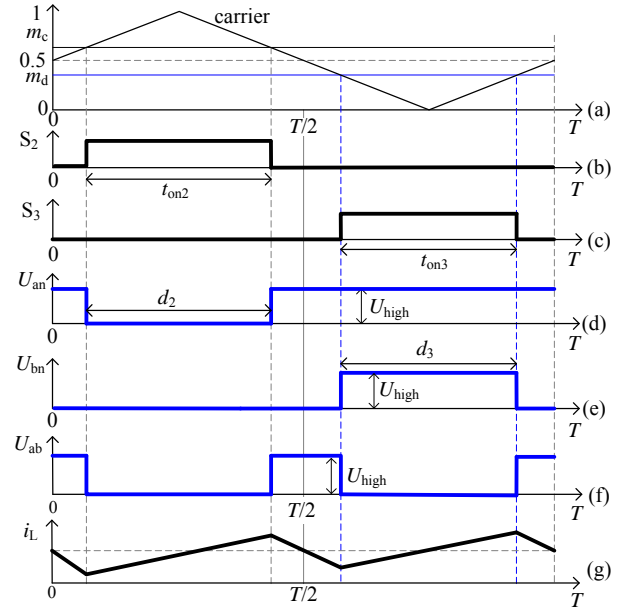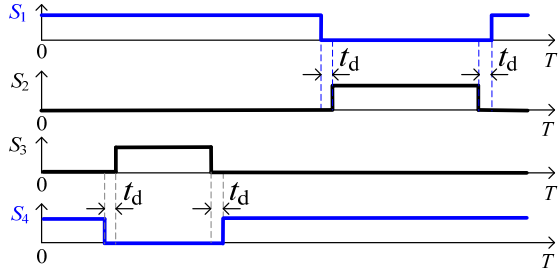### D. Synchronous Rectification Operation

Although the power semiconductors switch with duty cycles which are near 0.5, the inductor currents of the bidirectional H-Bridge converters have to flow in the corresponding anti-parallel diodes. However, this still lead to a lower efficiency, as well as lower utilization of the H-Bridge power switches. Therefore, a high ratio bidirectional DC-DC converter with a synchronous rectification H-Bridge is proposed in this paper. In addition, the H-Bridge is comprised of four MOSFETs Q_{D1}-Q_{D4} with anti-parallel diodes.
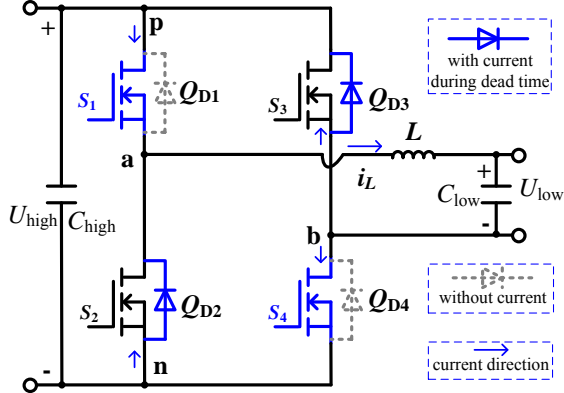
The synchronous rectification operation principle of the bidirectional H-Bridge is shown in Fig. 4. When it operates in the Buck mode (high ratio step-down), the main power semiconductors Q_{D1} and Q_{D4} switch according to the gate signals S_1 and S_4, as shown in Fig. 4(a). During the dead time t_d, the inductor current i_L flows into the anti-parallel diodes of Q_{D2} and Q_{D3}. Otherwise, by means of the gate signals S_2 and S_3, shown in Fig. 4(a), it flows into the controlled power switches Q_{D2} and Q_{D3}, as shown in Fig. 4(b). Similarly, when the bidirectional H-Bridge operates in the Boost mode (high ratio step-up), the main power semiconductors Q_{D2} and Q_{D3} switch according to the gate signals S_2 and S_3, shown in Fig. 4(c). In the dead time t_d, i_L flows into the anti-parallel diodes of Q_{D1} and Q_{D4}. Otherwise, in terms of the gate signals S_1 and S_4, shown in Fig. 4(c), it flows into the controlled power switches Q_{D1} and Q_{D4}, as shown in Fig. 4(d).

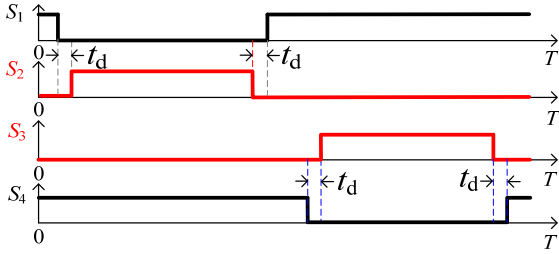### E. Control Strategy of Bidirectional Power Flow

Based on the operations analyzed in Section II (B-D), the bidirectional power flow control strategy can be achieved as shown in Fig. 5. When the bidirectional DC-DC converter interfaces with the battery stacks and the DC bus, it operates
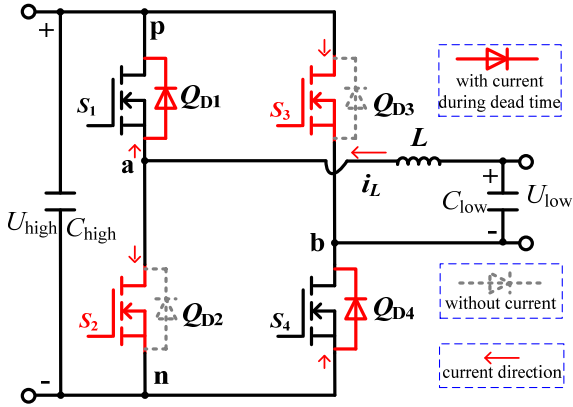
(a) Gate signals and dead time in Buck mode.

(b) Flowing paths of inductor current in Buck mode.

(c) Gate signals and dead time in Boost mode.

(d) Flowing paths of inductor current in Boost mode.

Fig. 4. Synchronous rectification operation principle of bidirectional H-Bridge.

as a current-source converter with a current loop. According to the power flow control signal U_c, the operation modes of the bidirectional DC-DC converter change between the step-down and the step-up modes. It operates in the step-down mode with U_c=0, and the inductor current i_L is controlled by the Buck current controller with the reference current $I_{ref\text{-}Buck}$. The corresponding PWM scheme, as shown in
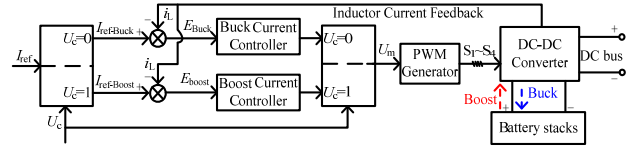

Fig. 5. Control strategy of bidirectional power flow.

Fig. 2 and Fig. 4(a), is selected to generate the gate signals S_1-S_4 in the step-down mode. Therefore, the power flow is from the DC bus to the battery stacks. During the step-down mode, if U_c is changed from "0" to "1", the inductor current i_L is controlled by the Boost current controller with the opposite direction reference current $I_{ref\text{-}Boost}$. The corresponding PWM scheme, as shown in Fig. 3 and Fig. 4(c), is selected to generate the gate signals S_1-S_4 in the step-up mode. As a result, the inductor current rises reversely after falling to zero. The power flow is controlled from the battery stacks to the DC bus.

III. SMALL-SIGNAL MODELING AND PARAMETERS DESIGN

A. Small-Signal Modeling

It is supposed that the power switches with anti-parallel diodes, the inductor, and the capacitors are ideal. The capacitance of C_{high} and C_{low} is large enough to neglect the voltage ripples.

When the bidirectional DC-DC converter operates in the step-up mode, the main power semiconductors Q_{D2} and Q_{D3} have three switching states: S_2S_3=[10, 00, 01]. When S_2S_3=10, its operation time is $d_2 \times T$, and the state space average model can be obtained as follows:

$$\begin{bmatrix} \dfrac{di_L(t)}{dt} \\ \dfrac{du_{high}(t)}{dt} \end{bmatrix}_{S_2S_3=10} = \begin{bmatrix} 0 & 0 \\ 0 & -\dfrac{1}{C_{high}R_{Boost}} \end{bmatrix} \begin{bmatrix} i_L(t) \\ u_{high}(t) \end{bmatrix} + \begin{bmatrix} \dfrac{1}{L} \\ 0 \end{bmatrix} u_{low}(t) \quad (8)$$

where R_{Boost} is the equivalent load resistance in the step-up mode. When S_2S_3=01, its operation time is $d_3 \times T$, and the state space average model can be written as:

$$\begin{bmatrix} \dfrac{di_L(t)}{dt} \\ \dfrac{du_{high}(t)}{dt} \end{bmatrix}_{S_2S_3=01} = \begin{bmatrix} 0 & 0 \\ 0 & -\dfrac{1}{C_{high}R_{Boost}} \end{bmatrix} \begin{bmatrix} i_L(t) \\ u_{high}(t) \end{bmatrix} + \begin{bmatrix} \dfrac{1}{L} \\ 0 \end{bmatrix} u_{low}(t) \quad (9)$$

When S_2S_3=00, its operation time is $(1-d_2-d_3) \times T$, and the state space average model can be achieved as:

$$\begin{bmatrix} \dfrac{di_L(t)}{dt} \\ \dfrac{du_{high}(t)}{dt} \end{bmatrix}_{S_2S_3=00} = \begin{bmatrix} 0 & -\dfrac{1}{L} \\ \dfrac{1}{C_{high}} & -\dfrac{1}{C_{high}R_{Boost}} \end{bmatrix} \begin{bmatrix} i_L(t) \\ u_{high}(t) \end{bmatrix} + \begin{bmatrix} \dfrac{1}{L} \\ 0 \end{bmatrix} u_{low}(t) \quad (10)$$

Combing (8), (9) and (10), the average model of the bidirectional DC-DC converter in the step-up mode can be obtained as (11).
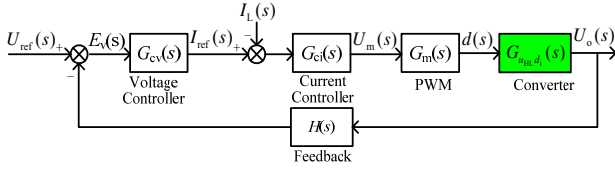
Fig. 6. Control scheme with voltage and current loops.

$$\begin{bmatrix} \dfrac{di_L(t)}{dt} \\ \dfrac{du_{high}(t)}{dt} \end{bmatrix} = \begin{bmatrix} 0 & -\dfrac{1-d_2(t)-d_3(t)}{L} \\ \dfrac{1-d_2(t)-d_3(t)}{C_{high}} & -\dfrac{1}{C_{high}R_{Boost}} \end{bmatrix} \begin{bmatrix} i_L(t) \\ u_{high}(t) \end{bmatrix} \quad (11)$$
$$+ \begin{bmatrix} \dfrac{1}{L} \\ 0 \end{bmatrix} u_{low}(t)$$

Based on (11), the small-signal disturbance variables $\hat{i}_L(t)$, $\hat{u}_{high}(t)$, $\hat{d}(t)$, and $\hat{u}_{low}(t)$ are introduced for the alternating current small-signal disturbance variables $i_L(t) = I_L + \hat{i}_L(t)$, $u_{high}(t) = U_{high} + \hat{u}_{high}(t)$, $d(t) = D + \hat{d}(t)$, and $u_{low}(t) = U_{low} + \hat{u}_{low}(t)$, respectively, where I_L, U_{high}, D and U_{low} are steady state components. In addition, $U_{high} = (1 - d_2(t) - d_3(t))I_L \times R_{Boost}$ and $U_{low} = U_{high} \times (1 - d_2(t) - d_3(t))$. As a result, the small-signal model of the bidirectional DC-DC converter in the step-up mode can be written as:

$$\begin{bmatrix} \dfrac{d\hat{i}_L(t)}{dt} \\ \dfrac{d\hat{u}_{high}(t)}{dt} \end{bmatrix} = \begin{bmatrix} 0 & -\dfrac{1-D_2-D_3}{L} \\ \dfrac{1-D_2-D_3}{C_{high}} & -\dfrac{1}{C_{high}R_{Boost}} \end{bmatrix} \begin{bmatrix} \hat{i}_L(t) \\ \hat{u}_{high}(t) \end{bmatrix} + \begin{bmatrix} \dfrac{1}{L} \\ 0 \end{bmatrix} \hat{u}_{low}(t)$$
$$+ \begin{bmatrix} 0 & \dfrac{1}{L} \\ -\dfrac{1}{C_{high}} & 0 \end{bmatrix} \begin{bmatrix} I_L \\ U_{high} \end{bmatrix} \hat{d}_2(t) + \begin{bmatrix} 0 & \dfrac{1}{L} \\ -\dfrac{1}{C_{high}} & 0 \end{bmatrix} \begin{bmatrix} I_L \\ U_{high} \end{bmatrix} \hat{d}_3(t) \quad (12)$$

According to (12), the dynamic mathematic model for the output disturbance variable $\hat{u}_{high}(s)$ and the control disturbance variables $\hat{d}_2(s)$ and $\hat{d}_3(s)$ in the step-up mode can be achieved from the time domain to the complex frequency domain as (13).

$$\begin{cases} G_{u_{high}d_2}(s) = \left.\dfrac{\hat{u}_{high}(s)}{\hat{d}_2(s)}\right|_{\hat{u}_{low}=0,\hat{d}_3(s)=0} = -\dfrac{I_L L s + U_{high}(D_2+D_3-1)}{LC_{high}s^2 + \dfrac{L}{R_{Boost}}s + (D_2+D_3-1)^2} \\ \\ G_{u_{high}d_3}(s) = \left.\dfrac{\hat{u}_{high}(s)}{\hat{d}_3(s)}\right|_{\hat{u}_{low}=0,\hat{d}_2(s)=0} = -\dfrac{I_L L s + U_{high}(D_2+D_3-1)}{LC_{high}s^2 + \dfrac{L}{R_{Boost}}s + (D_2+D_3-1)^2} \end{cases} \quad (13)$$

When the bidirectional DC-DC converter operates in the step-down mode, the main power semiconductors Q_{D1} and Q_{D4} have three switching states: $S_1S_4=[01, 10, 11]$. Similarly, the average model of the bidirectional DC-DC converter in the step-down mode can be achieved as (14).

$$\begin{bmatrix} \dfrac{di_L(t)}{dt} \\ \dfrac{du_{low}(t)}{dt} \end{bmatrix} = \begin{bmatrix} 0 & -\dfrac{1}{L} \\ \dfrac{1}{C_{low}} & -\dfrac{1}{C_{low}R_{Buck}} \end{bmatrix} \begin{bmatrix} i_L(t) \\ u_{low}(t) \end{bmatrix} \quad (14)$$
$$+ \begin{bmatrix} \dfrac{d_1(t)+d_4(t)-1}{L} \\ 0 \end{bmatrix} u_{high}(t)$$

where R_{Buck} is the equivalent load resistance in the step-down mode. Based on (14), the small-signal model of the bidirectional DC-DC converter in the step-down mode can be obtained as:

$$\begin{bmatrix} \dfrac{d\hat{i}_L(t)}{dt} \\ \dfrac{d\hat{u}_{low}(t)}{dt} \end{bmatrix} = \begin{bmatrix} 0 & -\dfrac{1}{L} \\ \dfrac{1}{C_{low}} & -\dfrac{1}{C_{low}R_{Buck}} \end{bmatrix} \begin{bmatrix} \hat{i}_L(t) \\ \hat{u}_{low}(t) \end{bmatrix} + \begin{bmatrix} \dfrac{D_1+D_4-1}{L} \\ 0 \end{bmatrix} \hat{u}_{high}(t)$$
$$+ \begin{bmatrix} \dfrac{D_1+D_4-1}{L} \\ 0 \end{bmatrix} U_{high}\hat{d}_1(t) + \begin{bmatrix} \dfrac{D_1+D_4-1}{L} \\ 0 \end{bmatrix} U_{high}\hat{d}_4(t) \quad (15)$$

In terms of (15), the dynamic mathematic model for the output disturbance variable $\hat{u}_{low}(s)$ and the control disturbance variables $\hat{d}_1(s)$ and $\hat{d}_4(s)$ in the step-down mode can be achieved from the time domain to the complex frequency domain as (16).

$$\begin{cases} G_{u_{low}d_1}(s) = \left.\dfrac{\hat{u}_{low}(s)}{\hat{d}_1(s)}\right|_{\hat{u}_{high}(s)=0,\hat{d}_4(s)=0} = \dfrac{U_{high}(D_1+D_4-1)}{LC_{low}s^2 + \dfrac{Ls}{R_{Buck}}+1} \\ \\ G_{u_{low}d_4}(s) = \left.\dfrac{\hat{u}_{low}(s)}{\hat{d}_4(s)}\right|_{\hat{u}_{high}(s)=0,\hat{d}_1(s)=0} = \dfrac{U_{high}(D_1+D_4-1)}{LC_{low}s^2 + \dfrac{Ls}{R_{Buck}}+1} \end{cases} \quad (16)$$

Based on (13) and (16), a control scheme with voltage and current loops can be obtained as shown in Fig. 6. When the bidirectional DC-DC converter operates in the step-up mode, the converter transfer function $G_{u_{HL}d_i}(s)$ is switched as (13). Otherwise, $G_{u_{HL}d_i}(s)$ is switched as (16). In addition, $G_m(s)$ is the PWM transfer function, $G_{cv}(s), G_{ci}(s)$ are the voltage and current controller transfer functions, and $H(s)$ is the feedback transfer function. Therefore, two PI (proportional integral) controllers can be designed for the bidirectional DC-DC converter to achieve static and dynamic performance.

B. Parameters Design of the Capacitor and Inductor

According to Fig. 1, Fig. 2 and the operation principle of the bidirectional DC-DC converter in the step-down mode, when $S_1S_4=11$, Q_{D1} and Q_{D4} are turned on, Q_{D2} and Q_{D3} are turned off, and the inductor is being charged. The charging time in each carrier period is $(d_1+d_4-1)\times T$, and the high frequency component current of the inductor current flows through the low voltage side capacitor. Then, (17) can be obtained as:

$$\begin{cases} \Delta U_{\text{low}} \times C_{\text{low}} = \dfrac{T}{4} \times \dfrac{\Delta I_{\text{L\_Buck}}}{2} \times \dfrac{1}{2} \\[3mm] L_{\text{Buck}} \dfrac{\Delta I_{\text{L\_Buck}}}{(D_1 + D_4 - 1)T/2} = U_{\text{high}} - U_{\text{low}} \end{cases} \quad (17)$$

where ΔU_{low} is the voltage ripple of the low voltage side capacitor, and $\Delta I_{\text{L\_Buck}}$ is the inductor current ripple in the step-down mode. In addition, $U_{\text{low}} = (D_1 + D_4 - 1)U_{\text{high}}$. Then the capacitance of the low voltage side capacitor and the inductance L_{Buck} in the step-down mode can be obtained as:

$$\begin{cases} C_{\text{low}} = \dfrac{\Delta I_{\text{L\_Buck}} \times T}{16 \Delta U_{\text{low}}} \\[3mm] L_{\text{Buck}} = \dfrac{U_{\text{low}}(2 - D_1 - D_4)T}{2 \Delta I_{\text{L\_Buck}}} \end{cases} \quad (18)$$

Similarly, in the step-up mode, the inductor is being discharged when $S_2 S_3 = 00$. The discharging time in each carrier period is $(1 - d_2 - d_3) \times T$. Then (19) can be achieved as:

$$\begin{cases} C_{\text{high}} \dfrac{\Delta U_{\text{high}}}{(1 - D_2 - D_3)T/2} = I_{\text{L\_Boost}} - I_{\text{o}} \\[3mm] L_{\text{Boost}} \dfrac{\Delta I_{\text{L\_Boost}}}{(1 - D_2 - D_3)T/2} = U_{\text{high}} - U_{\text{low}} \end{cases} \quad (19)$$

where ΔU_{high} is the voltage ripple of the high voltage side capacitor, and $\Delta I_{\text{L\_Boost}}$ is the inductor current ripple in the step-up mode. In addition, $I_{\text{o}} = (1 - D_2 - D_3)I_{\text{L\_Boost}}$ is the load current in the high voltage side, $U_{\text{low}} = (1 - D_2 - D_3)U_{\text{high}}$. Then the capacitance of the high voltage side capacitor and the inductance L_{Boost} in the step-up mode can be achieved as:

$$\begin{cases} C_{\text{high}} = \dfrac{I_{\text{o}}(D_2 + D_3)T}{2 \Delta U_{\text{high}}} \\[3mm] L_{\text{Boost}} = \dfrac{U_{\text{low}}(D_2 + D_3)T}{2 \Delta I_{\text{L\_Boost}}} \end{cases} \quad (20)$$

In terms of (18) and (20), the capacitance of the high and low voltage-side capacitors and the inductance of the inductor can be designed in this paper.

IV. EXPERIMENTAL VERIFICATION AND ANALYSIS

In experiments, the high voltage DC bus (supported by a high specific energy source, e.g. battery stacks) can be replaced by a constant DC voltage source with $U_{\text{high}} = 150\text{V}$ (as a stable input voltage), and the low voltage with a high specific power source (e.g. super-capacitors) can be replaced by a load resistor $R_{\text{Lbuck}} = 1.5 \sim 30\,\Omega$ or low voltage (48V) battery stacks in the Buck mode. In the Boost mode, the high specific power source (e.g. super-capacitors) can be replaced by an adjustable DC voltage source with a range of
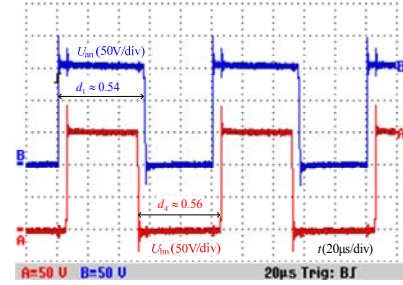
(a) Output PWM voltage of each half-bridge.
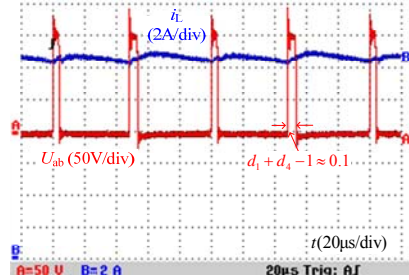
(b) Inductor current and output PWM voltage of H-Bridge.
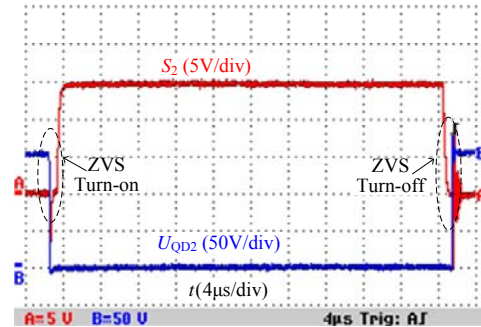
(c) Gate signal and voltage stress of synchronous rectification power switch.

Fig. 7. Output PWM voltages and inductor current with $M_{\text{Buck}} = 10$ in Buck mode.

$U_{\text{low}} = 15 \sim 50\text{V}$ (as a variable input voltage) or low voltage (48V) battery stacks, and the high DC bus voltage source (normally high specific energy source battery stacks) can be replaced by a load resistor $R_{\text{Lboost}} = 130 \sim 260\,\Omega$. In addition, the converter voltage loops are controlled by a TMS320F28335 DSP. For the power circuit IXTK102N30P MOSFETs are used. The switching frequency is $f_s = 10\text{kHz}$, the dead time is $t_d = 1\,\mu\text{s}$, and the initial value of the inductor is $L = 1.7\text{mH}$.

Fig. 7 and Fig. 8 show experimental results in the Buck mode. The output PWM voltages with $M_{\text{Buck}} = 10$ are shown in Fig. 7. In this mode, the output PWM voltages of each half-bridge U_{an} and U_{bn} are shown in Fig. 7(a). The output PWM voltage of the H-Bridge U_{ab}, shown in Fig. 7(b), is obtained from the voltage difference between U_{an} and U_{bn}. Although the step-down ratio is very high, a narrow pulse voltage U_{ab} still can be obtained by duty cycles that are near 0.5 (d_1 is about 0.54, and d_4 is about 0.56, as shown in Fig. 7(a)). In addition, the frequency of U_{ab} and the inductor
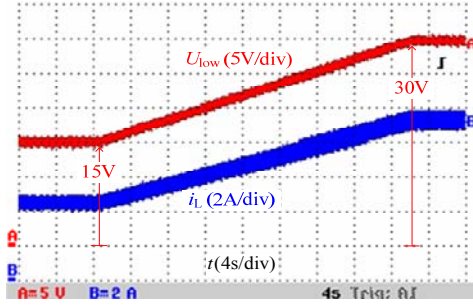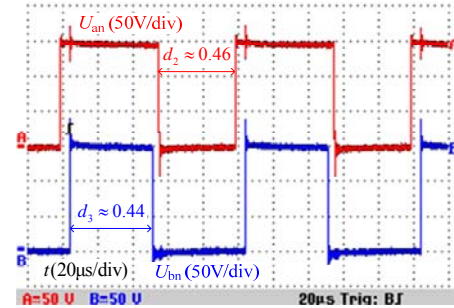
Fig. 8. Output voltage (varying from 15V to 30V) and the corresponding inductor current in Buck mode (R_{Lbuck}=1.5 Ω).

(a) Output PWM voltage of each half-bridge.

(b) Inductor current and output PWM voltage of H-Bridge.

(c) Gate signal and voltage stress of synchronous rectification power switch.

Fig. 9. Output PWM voltages and inductor current with M_{Boost}=10 in Boost mode.

Fig. 10. Input voltage (varying from 30V to 15V) and the corresponding output voltage in Boost mode (R_{Lboost}=130 Ω).

current i_L is double the switching frequency, because U_{ab} is indirectly obtained by the voltage difference between U_{an} and U_{bn}. The other two arms (Q_{D2} and Q_{D3}) operate in the freewheeling state with synchronous rectification. During the dead time, current flows through the anti-parallel diodes of Q_{D2} and Q_{D3}, leading to near zero voltage stress. Otherwise, the freewheeling current is turned on or turned off by the controlled MOSFETs Q_{D2} and Q_{D3} with ZVS (zero voltage switching), as shown in Fig. 7(c).
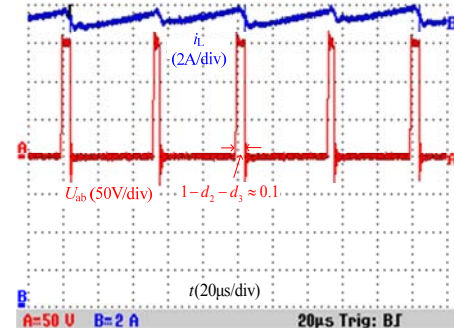
In Fig. 8, the load resistor for the Buck mode is R_{Lbuck}=1.5 Ω , and the output voltage U_{low} is controlled from 15V to 30V with a variable reference voltage in a few seconds. And the inductor current i_L increases correspondingly until the output voltage arrives at U_{low}=30V. In this dynamic process, the converter steps down with synchronous rectification in a wide range of 5~10.

Fig. 9 and Fig. 10 show experimental results in the Boost mode with a load of R_{Lboost}=50~130 Ω . The output PWM voltages with M_{Boost}=10 are shown in Fig. 9. The output PWM voltages U_{an} and U_{bn} of each half-bridge with wider duty cycles are shown in Fig. 9(a). In this mode, Q_{D2} and Q_{D3} alternate to be the main power switches, and Q_{D1} and Q_{D4} become the rectification power switches. Then the output narrow PWM voltage U_{ab} is obtained from the voltage difference between U_{an} and U_{bn}, as shown Fig. 9(b). Similarly, the frequencies of U_{ab} and i_L are double the switching frequency. It can be seen that the high step-up ratio can still be achieved by the duty cycles of the main power switches, which are near 0.5 (d_2 is about 0.46, and d_3 is about 0.44, as shown in Fig. 9 (a)). For Q_{D1} and Q_{D4}, current flows through the anti-parallel diodes of Q_{D1} and Q_{D4} during the dead time. Then, their blocking voltages are around zero. Otherwise, the current is turned on or turned off by the controlled MOSFETs Q_{D1} and Q_{D4} with ZVS, as shown in Fig. 9(c).
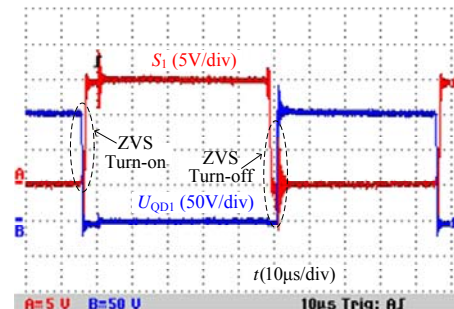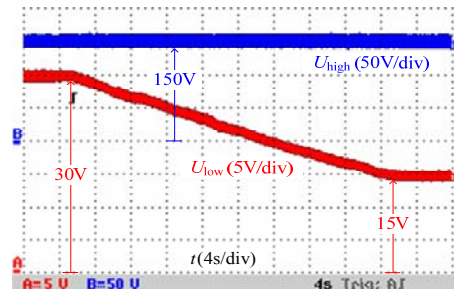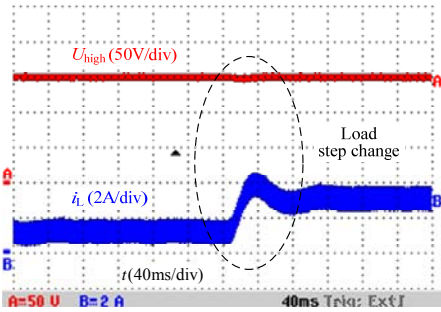
The input voltage and step-up output voltage are shown in Fig. 10. The reference voltage is given at 150V, and the input voltage continuously varies from 30V to 15V. However, the corresponding output voltage is stable at 150V. Therefore, a constant output voltage of 150V can be obtained by the variable input DC voltage source and the wide range voltage-gain of 5-10.

The output voltages and inductor currents under load step changes from the bidirectional DC-DC converter are shown in Fig. 11. In the step-down mode, the output voltage U_{low} is controlled at 50V, and the load resistor is changed from 15 Ω to 30 Ω with a load step change. The inductor current i_L changes from 3.3A to 1.65A, and the output voltage U_{low} is
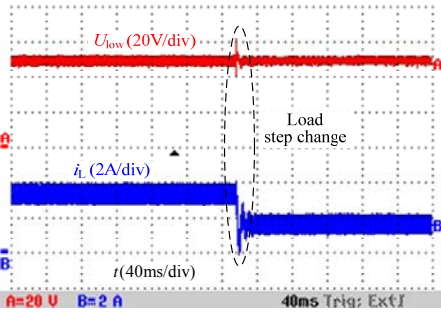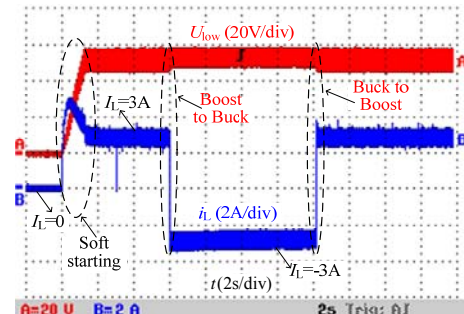
(a) In step-down mode.

(b) In step-up mode.

Fig. 11. Output voltages and inductor currents under load step change.

(a) Process of soft starting, Boost to Buck, and Buck to Boost.

(b) Transient process of Buck to Boost.

Fig. 12. Experimental results of bidirectional power flow control.

Fig. 13. Efficiency comparisons between diode and synchronous rectification operations for proposed bidirectional converter. (U_{high}=150V, U_{low}=15~50V, R_{Lbuck}=6 Ω , R_{Lboost}=130 Ω).
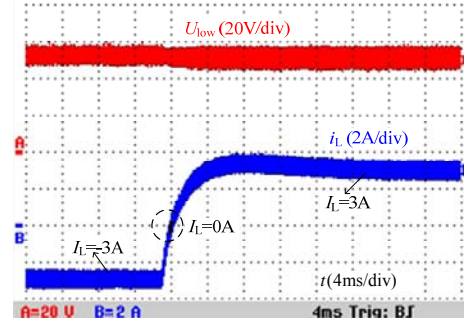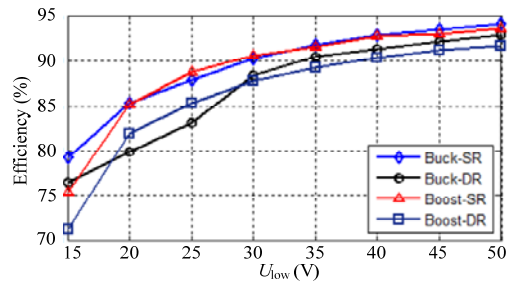
stabilized at 50V after approximately 30ms, as shown in Fig. 11(a). In the step-up mode, the output voltage U_{high} is controlled at 150V. The load resistor is changed from $100\,\Omega$ to $50\,\Omega$ with a load step change, the inductor current i_L changes from 1.5A to 3A, and the output voltage U_{high} is stabilized at 150V after approximately 80ms as shown in Fig. 11(b).

In order to validate the bidirectional power control scheme, some experimental results are shown in Fig. 12. Low voltage battery stacks (48V) and a high voltage DC bus (150V) interface with the proposed bidirectional DC-DC converter. In Fig. 12(a), when the converter starts, the soft starting process is needed to suppress the rush current in the inductor. Then the converter operates at the reference inductor current $I_{ref-Boost}$=3A with a current control loop in the step-up mode, and there is a power flow from the low voltage battery stacks to the high voltage DC bus. When the power flow needs to be changed, the converter operates at the reference inductor current $I_{ref-Buck}$=-3A, and the inductor current rises reversely after falling to zero (Boost to Buck). The converter operates at the reference inductor current $I_{ref-Buck}$=-3A in the step-down mode, and the power flow goes from the high voltage DC bus to the low voltage battery stacks. Similarly, the converter can also switch from the step-down mode to the step-up mode (Buck to Boost), and the transient process is shown in Fig. 12(b). The inductor current falls to zero from I_L=-3A. Then it increases and stabilizes at I_L=3A in approximately 20ms.

In addition to the high ratio bidirectional step-down and step-up operations of the proposed converter, the synchronous rectification operation, which takes advantage of

the proposed topology instead of extra hardware, improves the efficiency as well as the utilization of the freewheeling and rectification power switches. When U_{high} is a constant 150V, and the output voltage (in the Buck mode) varies from 15V to 50V, or the input voltage (in the Boost mode) varies from 50 to 15V, the efficiencies measured by a power analyzer (Yokogawa-WT3000) are compared between the DR and SR operations for the proposed bidirectional converter and are shown in Fig. 13.

In the step-down mode, when the bidirectional DC-DC converter operates with the diode rectification (DR), the discharging inductor current flows through one MOSFET and one diode in series, while it flows through two MOSFETs in series with the SR operation. In addition, the on-resistance of the selected MOSFET is less than its anti-parallel diode, as well as the ZVS operation of the SR power switches. Therefore, the efficiency (Buck-SR) with the SR operation is higher than that (Buck-DR) with the DR operation, as shown in Fig. 13. In the step-up mode with the DR operation, the

discharging inductor current flows through two diodes in series, and the charging inductor current flows through one MOSFET and one diode in series, while the inductor current flows through two MOSFETs in series with the SR operation. Similarly, the efficiency (Boost-SR) with the SR operation is higher than that (Boost-DR) with the DR operation, as shown in Fig. 13. Because the flowing path of the inductor current is devolved from the anti-parallel diodes to the controlled MOSFETs, the efficiencies in the Buck and Boost modes are improved by 4.8% and 3.4%, respectively. When U_{low} continuously varies between 15V and 50V, the maximum efficiency arrives at 94.1% and 93.6% in the Buck-SR and Boost-SR operations, respectively.

V. CONCLUSIONS

A high ratio bidirectional DC-DC converter with a synchronous rectification H-Bridge is proposed in this paper, and the high ratio bidirectional operations can be obtained by non-extreme duty cycles that are near 0.5. In addition, the equivalent switching frequency is double the actual one, and the bidirectional synchronous rectification operations are achieved by taking full advantage of the H-Bridge, instead of extra hardware. Then compared with the diode rectification, the power conversion efficiency is improved significantly when the low voltage side voltage varies widely. Therefore, it is suitable for application as a power interface between the battery and super-capacitor stacks in hybrid energy sources electric vehicles.

REFERENCES

[1] K. Li, T. Chen, Y. Luo, and J. Wang, "Intelligent environment-friendly vehicles: Concept and case studies," *IEEE Trans. Intell. Transp. Syst.*, Vol. 13, No. 1, pp. 318-328, Mar. 2012.

[2] A. Y. Saber and G. K. Venayagamoorthy, "Efficient utilization of renewable energy sources by gridable vehicles in cyber-physical energy systems," *IEEE Syst. J.*, Vol. 4, No. 3, pp. 285-294, Sep. 2010.

[3] A. Gholami, J. Ansari, M. Jamei, and A. Kazemi, "Environmental/economic dispatch incorporating renewable energy sources and plug-in vehicles," *IET Gener. Transm. Distrib.*, Vol. 8, No. 12, pp. 2183-2198, May 2014.

[4] J. X. Jin, X. Y. Chen, and L. Wen, S. C. Wang, and Y. Xin, "Cryogenic power conversion for SMES application in a liquid hydrogen powered fuel cell electric vehicle," *IEEE Trans. Appl. Supercond.*, Vol. 25, No. 1, article #. 5700111, Feb. 2015.

[5] K. Maalej, S. Kelouwani, and K. Agbossou, Y. Dube, and N. Henao, "Long-trip optimal energy planning with online mass estimation for battery electric vehicles," *IEEE Trans. Veh. Technol.*, Vol. 64, No. 11, pp. 4929-4941, Nov. 2015.

[6] A. Y. Saber and G. K. Venayagamoorthy, "Plug-in vehicles and renewable energy sources for cost and emission reductions," *IEEE Trans. Ind. Electron.*, Vol. 58, No. 4, pp. 1229-1238, Apr. 2011.

[7] U. R. Prasanna, X. Pan, A. K. Rathore, and K. Rajashekara, "Propulsion system architecture and power conditioning topologies for fuel cell vehicles," *IEEE Trans. Ind. Appl.*, Vol. 51, No. 1, pp. 640–650, Jan./Feb. 2015.

[8] A. Tani, M. B. Camara, and Brayima Dakyo, and Y. Azzouz, "DC/DC and DC/AC converters control for hybrid electric vehicles energy management-ultracapacitors and fuel cell," *IEEE Trans. Ind. Inf.*, Vol. 9, No. 2, pp. 686–696, May 2013.

[9] J. Ko, S. Ko, and H. Son, B. Yoo, J. Cheon, and H. Kim, "Development of brake system and regenerative braking cooperative control algorithm for automatic-transmission-based hybrid electric vehicles," IEEE Trans. *Veh. Technol.*, Vol. 64, No. 2, pp. 431-440, Feb. 2015.

[10] X. Nian, F. Peng, and H. Zhang, "Regenerative braking system of electric vehicle driven by brushless DC motor," *IEEE Trans. Ind. Electron.*, Vol. 61, No. 10, pp. 5798-5808, Oct. 2014.

[11] J. P. F. Trovão, V. D. N. Santos, and C. H. Antunes, P. . Pereirinha, and H. M. Jorge, "A real-time energy management architecture for multisource electric vehicles," *IEEE Trans. Ind. Electron.*, Vol. 62, No. 5, pp. 3223-3233, May 2015.

[12] A. Kuperman, I. Aharon, S. Malki, and A. Kara, "Design of a semiactive battery-ultracapacitor hybrid energy source," *IEEE Trans. Power Electron.*, Vol. 28, No. 2, pp. 806-815, Feb. 2013.

[13] P. Thounghong, B. Davat, and S. Rael, "Drive friendly," *IEEE Power and Energy Magazine*, Vol. 6, No. 1, pp. 69-76, Jan./Feb. 2008.

[14] Z. Amjadi and S. S. Williamson, "Digital control of a bidirectional DC/DC switched capacitor converter for hybrid electric vehicle energy storage system applications," *IEEE Trans. Smart Grid*, Vol. 5, No. 1, pp. 158-166, Jan. 2014.

[15] G. Su and L. Tang, "A multiphase, modular, bidirectional, triple-voltage DC–DC converter for hybrid and fuel cell vehicle power systems," *IEEE Trans. Power Electron.*, Vol. 23, No. 6, pp. 3035-3046, Nov. 2008.

[16] T. Bhattacharya, V. S. Giri, K. Mathew, and L. Umanand, "Multiphase bidirectional flyback converter topology for hybrid electric vehicles," *IEEE Trans. Ind. Electron.*, Vol. 56, No. 1, pp. 78-84, Jan. 2009.

[17] A. Purwadi, K. A. Nugroho, A. Rizqiawan, and P. A. Dahono, "A new approach to synthesis of static power converters," in *Conf. ICEEI 2009*, pp. 627-632, 2009.

[18] A. Purwadi, K. A. Nugroho, F. Sasongko, K. F. Sutrisna, and P. A. Dahono, "Performance evaluation and control technique of large ratio DC-DC converter," in *Conf. ICEEI 2009*, pp. 633-639, 2009.

Yun Zhang (M'13) was born in Jiangsu, China. He received his B.S. and M.S. degrees from the Harbin University of Science and Technology, Harbin, China, in 2003 and 2006, respectively; and his Ph.D. degree from the Harbin Institute of Technology, Harbin, China, in 2010, all in Electrical Engineering. In 2010, he became a Lecturer in the School of Electrical Engineering and Automation, Tianjin University, Tianjin, China, where he is presently working as an Associate Professor. His current research interests include topologies, and the modulation and control strategies for the power converters of microgrids and electric vehicles.

Yongping Gao was born in Shanxi, China. He received his B.S. degree in Electrical Engineering from the China University of Mining and Technology, Xuzhou, Jiangsu, China, in 2015. He presently working towards his M.S. degree in Electrical Engineering from Tianjin University, Tianjin, China. His current research interests include power electronics converters, and energy management.

Jing Li (M'15) was born in Beijing, China. She received her B.S. (Honors) and M.S. (Distinction) degrees from the Beijing Institute of Technology, Beijing, China, in 1999, and 2002, respectively; and her Ph.D. degree from the University of Nottingham, Nottingham, England, UK, in 2010. She subsequently worked as a Research Fellow in the Power Electronic, Machine and Control Group (PEMC) in the University of Nottingham. She is presently working as a Lecturer in the Department of Electrical and Electronic Engineering, University of Nottingham, Ningbo, China. Her current research interests include the condition monitoring of motor drive systems and power distribution systems, advanced control and the design of motor drive systems.

Mark Sumner (SM'05) received his B.S. degree in Electrical and Electronic Engineering from Leeds University, Leeds, England, UK, in 1986; and his Ph.D. degree in Induction Motor Drives from the University of Nottingham, Nottingham, England, UK, in 1990. In 1986, he worked for Rolls Royce Ltd., Ansty, England, UK. In 1990, he worked as a Research Assistant at the University of Nottingham. In 1992, he became a Lecturer and he is presently working as a Professor of Electrical Energy Systems. His current research interests include the control of power electronic systems including sensorless motor drives, the diagnostics and prognostics for drive systems, power electronics for enhanced power quality and novel power system fault location strategies.

Ping Wang was born in Tianjin, China, in 1959. She received her B.S., M.S., and Ph.D. degrees in Electrical Engineering from the Tianjin University, Tianjin, China, in 1981, 1991, and 2005, respectively. Since 1981, she has been a Teacher and a Researcher at Tianjin University, where she is presently working as a Professor. Her current research interests include the power electronics control of renewable energy sources, PWM converters, and intelligent detection and control.

Lei Zhou was born in Ningxia, China. He received his B.S. degree in Electrical Engineering from Tianjin University, Tianjin, China, in 2015, where he is presently working towards his M.S. degree in Electrical Engineering. His current research interests include DC-DC converters, and the modeling and analysis of DC-DC converters.